Effects of Bionic Volute Tongue Bioinspired by Leading Edge of Owl Wing and Its Installation Angle on Performance of Multi-Blade Centrifugal Fan

X. Dong and H. S. Dou[†]

Faculty of Mechanical Engineering and Automation, Zhejiang Sci-Tech University, Hangzhou, Zhejiang 310018, China

†*Corresponding Author Email: huashudou@yahoo.com*

ABSTRACT

Effect of the volute tongue of the multi-blade centrifugal fan on the performance of the machines is significance. The shape and installation angle of the volute tongue affect the circulating internal flow behavior of the volute as well as the energy loss around the volute tongue. In this study, the profile of the leading edge of the owl wing is applied to the volute tongue of a multi-blade centrifugal fan to improve the aerodynamic performance of the fan. The fan models with different volute tongue installation angles are numerically simulated under different flow conditions. The research results show that the proposed design is able to improve the aerodynamic performance of the fan at different flow rate conditions. In addition, an improved method for quantitatively evaluating the level of impeller-volute tongue interaction based on the unsteady simulation result is proposed and it is verified to be effective. Furthermore, the two parameters for evaluating the internal flow circulation which are influenced by the installation angle of the bionic volute tongue are analyzed, namely the recirculated flow coefficient and the reversed flow coefficient. Combined with the analysis of energy loss around the volute tongue, the mechanism of variation of the aerodynamic performance of the multi-blade centrifugal fan with different volute tongue installation angles is explained.

Keywords: Multi-blade centrifugal fan; Bionic design; Numerical simulation; Internal flow circulation.

1. INTRODUCTION

The remarkable feature of multi-wing centrifugal fan are that the diameter ratio of inlet and outlet is larger than 0.8, the width-diameter ratio is larger than 0.25, the blades are short and simple in shape (usually single-arc or double-arc shaped blades, and the thickness of blades is constant), and a large number of blades for impeller (Gou and Kim 2003). Because of its low noise and small size, it is widely used in household appliances such as air conditioners and exhaust fume exhausters. The double-suction multi-blade centrifugal fan has the advantages of large flow rate and compact structure.

The role of the volute is to guide the air leaving the impeller to the volute outlet. The volute tongue can prevent part of the gas from circulating into the volute. Kawaguchi *et al*. (1994) visualized the flow field near the impeller using spark tracing method, showing the recirculation of air inside the fan, and found that the recirculation is more evident near the volute tongue. Kind and Tobin (1990) visualized the

flow field in a multi-blade centrifugal fan. It is observed that flow patterns are complex and there is reverse flow through the impeller even at the best-efficiency operating condition. Wang *et al*. (2018) quantitatively described the complex flow at the impeller inlet and outlet through numerical calculation. It is observed that the reverse flow at the impeller inlet and outlet occurs near the volute tongue. All the above shows that the flow around the volute tongue is very complicated.

Owls are well-known for their silent flight characteristics, Graham (1934) pointed out that although owls are a little lighter than eagles, they generated much less noise during flight because they can slowly flap their wings to make the angle of incidence small. For improvement of aerodynamic performance, the application of the owl wing airfoil has also generated evident results. Klan *et al*. (2009) based on the Birnbaum–Glauert function to reconstruct and modify the scanned owl airfoil line, and arranged the velvet on the airfoil surface. Experiments results showed that the presence of

velvet can reduce the formation of separation vortices. Wang *et al.* (2019) proposes an airfoil inspired by the long-eared owl wing and another airfoil coupled with leading edge waves and trailing edge serration. The Numerical simulation results showed that couple airfoil application is effective to reducing noise and improving lift-to-drag ratio. Li and Liu (2016) extracted and analyzed the aerodynamic characteristics of the long-eared owl wings at different spanning positions, whose thickness gradually decreased from the wing root to the wing tip. The airfoil leading edge pressure distribution at the wing root is relatively uniform regardless of the angle of attack of 0 ° or 5 °.

In recent years, many scholars have applied the bionic volute tongue to the fan. Sun *et al.* (2008) and Sun (2009) studied the impact of the volute tongue on the internal flow inside a fan. It was pointed out that the noise reduction mechanism of the bionic system was mainly obtained by reducing the impact of the airflow on the volute tongue, weaken the pressure fluctuation of the turbulent boundary layer on the surface of the volute tongue and delay the separation and shedding of the vortex flow behind the volute tongue. Liu and Li (2015) applied the profile of long-eared owl airfoil to the design of the volute tongue profile of the fan, the aerodynamic performance of the fan has been improved, and the noise has been reduced to a certain extent. Wang *et al.* (2017) pointed out that the bionic technology of the volute tongue based on the leading edge of the long-eared owl can effectively alleviate the flow separation phenomenon near the volute tongue.

In this paper, we take a multi-blade centrifugal fan as the prototype, carry out numerical simulation, and apply the bionic volute tongue to improve the aerodynamic performance of the volute tongue, which is extracted from the leading edge of owl wing. The performance of the fan under different installation angles and flow rates was studied, and the internal flow field is analyzed to explore the mechanism for the influence of the internal flow on the aerodynamic performance.

2. DESCRIPTION OF CENTRIFUGAL FAN

A model of double-suction multi-blade centrifugal fan is taken as the research prototype, and the structure and geometric parameters of the fan are shown in Fig. 1 and Table 1. The rated speed of the impeller is n=630r/min, and the design volume flow of the fan is Q=3.54m³/s.

3. NUMERICAL METHOD

3.1 Computational Model and Meshing

The fan was modeled by Solid works software and meshed by ICEM software. The fluid region is divided into four parts, namely the inlet part, the volute part, the impeller part, and the outlet part, where the inlet and outlet extended by a length of four times of D_2. Each domain consists of the elements of structured hexahedral grid, whose quality both are above 0.5. The grids of impeller and

volute tongue regions were appropriately refined and the value of Y+ is controlled within 60. The grid of impeller and volute tongue is shown in Figs. 2(a) and 2(b), respectively, and the grid of the entire model is shown in Fig. 2(c).
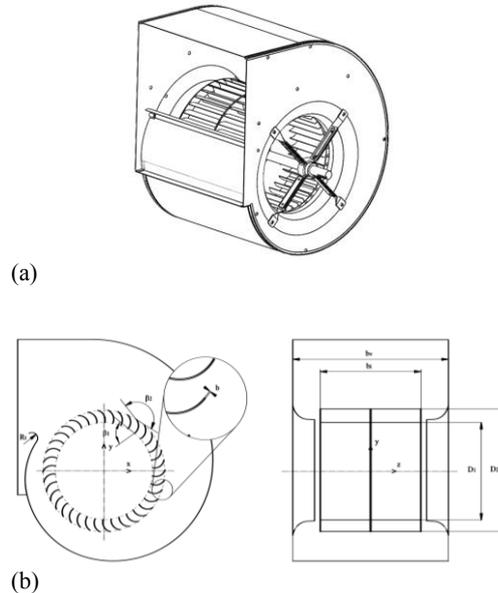

(a)

(b)

Fig. 1. Fan configuration: (a) structure of the fan, (b) geometric parameters of the fan.

Table 1 General Parameters of the fan

Parameter	Value
Number of blades, z	38
Impeller inlet diameter, D_1	396mm
Impeller outlet diameter, D_2	502mm
Impeller width, b_i	400mm
Blade width, b	1.2mm
Blade outlet angle, β_2	160.1°
Blade inlet angle, β_1	74.8°
Outlet area, A_{out}	0.407m²
Nozzle throat area, A_{in}	0.337m²
Volute width, b_v	634mm
Volute tongue radius, R_t	22mm

To ensure the accuracy of the calculation and to reduce the calculation time, the grid independence verification had been first performed. The total pressure and the efficiency of the fan are calculated by the formula

$$P_t = P_{out} - P_{in} \tag{1}$$

$$\eta = 9.549 \frac{P_t Q}{Mn} \tag{2}$$

where P_{out} and P_{in} are the total pressure at the outlet and the inlet of fans, respectively, M is the torque of the fan shaft in unit of N·m.

(a)

(b)

(c)
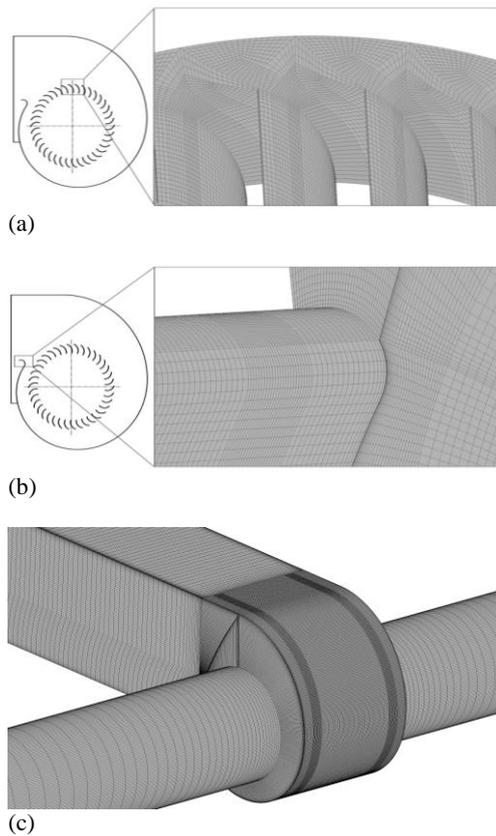
Fig. 2. Grid division: (a) grid of impeller, (b)grid of volute tongue , (c) grid of whole fan.

The verification result is shown in Fig. 3. When the elements number of grid is more than 9.6 million, an increase of 1.24 million elements, the total pressure and efficiency are only changed by 0.35% and 0.26%, respectively. So the final elements number of grid we chose is 9.6 million, The elements number of the impeller part, the volute part, the inlet part, and the outlet part are 4.7 million, 3.06 million, 1.14 million, and 0.7 million, respectively.
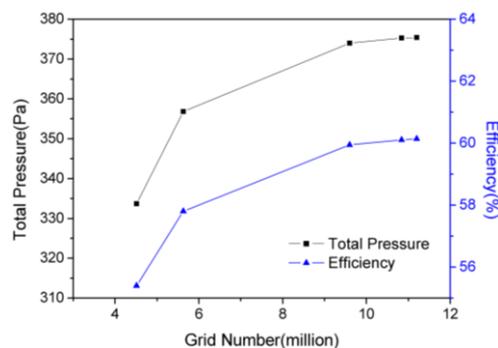
Fig. 3. Independence verification of grid.

3.2 Computational Setup

Numerical simulation of multi-blade centrifugal fans was performed by a commercial software of CFD, namely CFX. The fluid medium in the fan is air, the density is 1.185kg/m^3, and the dynamic viscosity is 1.831×10^{-5}kg/m·s. The Mach number of impeller

exit is $2D_2\pi n/60c$ =0.098<0.3, where c is local sound speed. Thus, an incompressible fluid was used in this case, and the energy equation was not considered. The flow field was simulated by solving the Navier-Stokes equation through the finite volume method. Moreover, the RNG k-ε model with the scalable wall function was used, which has a considerable result in numerical simulation of the fan (Darvish and Frank 2012; Bouhelal *et al*. 2018).

For the steady numerical simulation, ensuring the accuracy of calculation (Dong and Li (2020), Peng *et al*. 2020; Li *et al*. 2019), the advection term is approximated by the second-order upwind scheme. The criterion of convergence is set as the value of the mass residual to be 10^{-5} (Supreeth *et al*. 2020). Between the rotating and stationary domains, the frozen rotor interface was adopted. Mass flow and average static pressure boundary conditions were applied to the inlet and outlet, respectively.

For unsteady numerical simulation, the results of the steady simulation were used as the initial values. The second-order backward Euler difference format was adopted for the transient calculation. The interface between the rotating and stationary domain had been changed to a transient frozen rotor interface. Other boundary conditions are same as those in the steady simulation. Figure 4(a) shows the average pressure difference between three pairs of monitoring points at the inlet and the outlet part in a calculation time. Since the range of pressure fluctuation is small after five rounds, numerical simulation results after five rounds were chosen in this study. In order to select a time step that is both accurate in numerical simulation results and economical in numerical simulation time, the independence verification of time step was performed in time steps of 1251μs, 626μs, 313μs, and 209μs. Figure 4(b) shows that when the time step is less than 313μs, the relative difference of the total pressure and efficiency of the fan is less than 0.03%, which has little effect on the numerical simulation result. Therefore, the time step of 313μs has been selected.

3.3 Experimental Verification

In order to ensure the accuracy of the numerical simulation results, total pressure and efficiency obtained by numerical simulation were compared with the experimental results. The experiment was carried out at the experimental rig at Zhejiang Yilida Ventilator Co. Ltd. Figure 5 and Fig. 6 show the experiment set-up and the result of the comparison, respectively. The measurement devices are listed in the caption of Fig.5.The efficiency curves are almost consistent. The total pressure curve is in good agreement with the experiment in large flow rate conditions. In the case of small flow rate conditions, the total pressure curve of experimental results has a dipping trend from the design flow rate to small flow rate. However, the total pressure of simulation result has a slight increase, which is consistent with the characteristics of the increase in pressure due to the airflow not filling the whole blade path in the small flow rate condition (Cheng 2011). The pressure of the experimental data is a result of multi-point average, which is greatly affected by the position of

the measuring point and other factors. Besides, the deviations caused by the simplification of the fan model and the deformation of the blade are can't be ignored as well in terms of numerical simulation results. The exact comparison of experimental and numerical simulation results needs to be further explored. In summary, the numerical simulation results can provide a reference about the design and improvement of the fan.
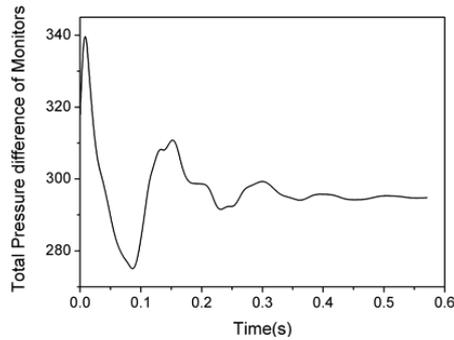
(a)
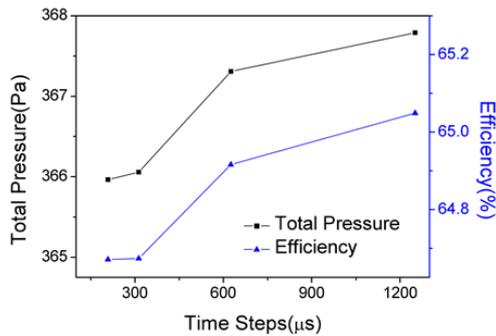
(b)

Fig. 4. Independence verification of calculation time: (a) time-total pressure difference curve of monitors, (b) independence verification of calculation time.

4.   DESIGN OF BIONIC VOLUTE TONGUE

According to the method given in the literature (Liu *et al*. 2006), the relationship between the upper and lower surface and the mean camber line of the airfoil is

$$z_{upper} = z_{(c)} + z_{(t)} \qquad (3)$$

$$z_{lower} = z_{(c)} - z_{(t)} \qquad (4)$$

Where z_{upper} and z_{lower} are the coordinates of the upper surface and lower surface of the airfoil, and $z(c)$ is the coordinate of mean camber line.
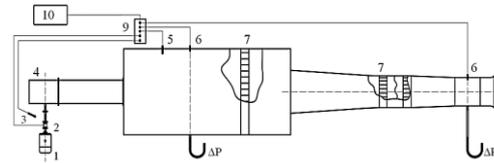
In order to extract the mean camber line, the Birnbaum-Glauert curve function is used

$$\frac{z_{(c)}}{c} = \frac{z_{(c)max}}{c} \lambda(1-\lambda) \sum_{n=1}^{3} S_n (2\lambda-1)^{n-1} \qquad (5)$$
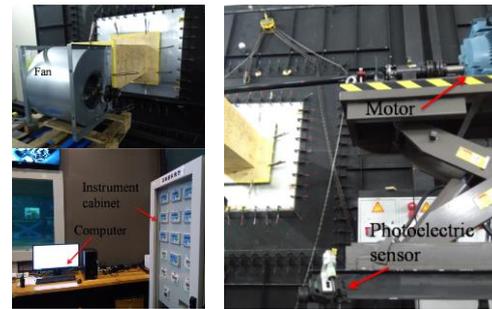
where $\lambda = x/c$ is the chord coordinate ratio, $z_{(c)max}$ is the coordinate of maximum camber, c is the local wing chord, and S_n is the undetermined coefficient.

The thickness distribution is given by

$$\frac{z_{(t)}}{c} = \frac{z_{(t)max}}{c} \lambda(1-\lambda) \sum_{n=1}^{4} A_n (\lambda^{n+1} - \sqrt{\lambda}) \qquad (6)$$
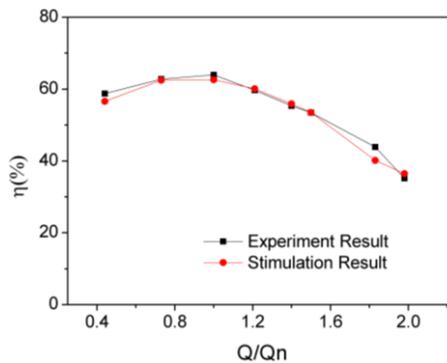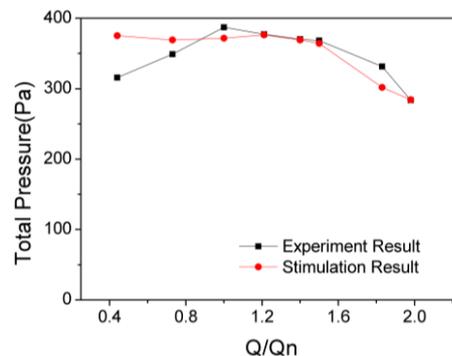

(a)

(b)

Fig. 5. Experimental set-up: (a) Sketch of the experimental set-up, (b) Photographs of the experimental equipment. 1. Electric motor, 2. Coupling, 3.Photoelectric sensor, 4. Test fan, 5. Temperature and humidity sensor, 6.Pressure sensor, 7. Flow regulation device, 8. Taper nozzle, 9.Data acquisition system, 10.Personal computer.

(a)

(b)

Fig. 6. Comparisons of efficiency and total pressure between the experimental and numerical simulation result: (a) Comparison of efficiency (b) Comparison of total pressure.

Table 2 General Parameters of the fan

Coefficient	n=1	n=2	n=3	n=4
Sn	3.88542	-1.39318	-0.62873	--
An	8.66355	-135.368	-290.022	-166.24

where $z_{(t)max}$ is the coordinate of maximum thickness, A_n is the undetermined coefficient.

According to the leading edge airfoil data of the owl wing at 40% wingspan given in literature (Sun 2008), four points of airfoil have been extracted to solve the coefficients S_n, A_n in equations (5) and (6), and the coefficients results are shown in Table 2.

According to the coefficients in table 2, the first 18% chord length of the airfoil fitting line had been drawn, as shown in Fig. 7(a). In this study, the first 15% chord length of the fitting line of airfoil had been employed for the bionic design of the volute tongue. By adjusting the ratio of the extracted line, the change of spiral part of the fan volute was minimized. Besides, the first-order geometric continuation between the volute tongue profile and spiral part of the fan volute profile was ensured.

It has been point out in book (Cheng 2011) that the deeper the volute tongue, the shorter length of the clearance between the volute and the impeller exit (the volute tongue clearance), and the smaller leakage flow between the spiral part of the volute and the volute outlet. That is beneficial to improve the efficiency and pressure of the fan, but is not conducive to the reduction of noise. Ensuring no increase of the noise value theoretically, the constant of the area of the volute outlet and the depth of volute tongue has been guaranteed in this study. The comparison of volute between the final designed BVT1 model and the original model is shown in Fig. 7(b), and the length of volute tongue clearance of BVT1 model is increased by 4.6 mm compared with the original model.

With the improved design of the volute tongue profile, the tip radius of the volute tongue and the length of volute tongue clearance are also changed accordingly. The reduction in tip radius of the volute tongue and the shortening of volute tongue clearance can increase noise, but the latter is much more influential than the former (Cheng 2011).Ensuring the no increase of the noise value theoretically, the length of the volute tongue clearance of following designed models has not been reduced.

In order to study the effects of different installation angles of the bionic volute tongue and its corresponding length of volute tongue clearance on the performance of the fan, on the basis of the BVT1 model, the bionic volute tongue is rotated. The appropriate adjustment ensures the first-order geometric continuity of the volute profile and the constant of volute exit area. Compared with original model, the BVT2 model obtained by turning the volute tongue clockwise by 6° has an increase of 0.6 mm in length of the volute tongue clearance, while the BVT3 model obtained by counterclockwise

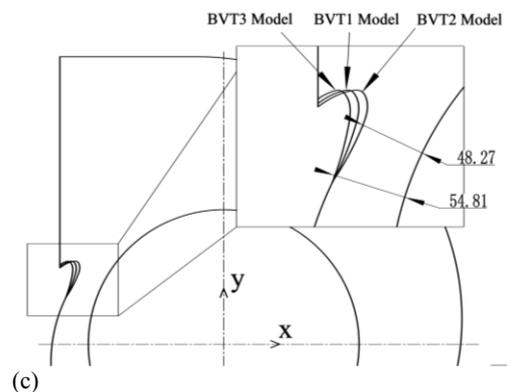rotation of 6° has an increase of 7.1 mm. A comparison of the three designed models is shown in Fig. 7(c).
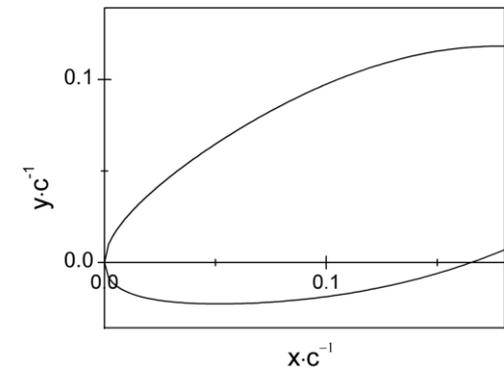
(a)
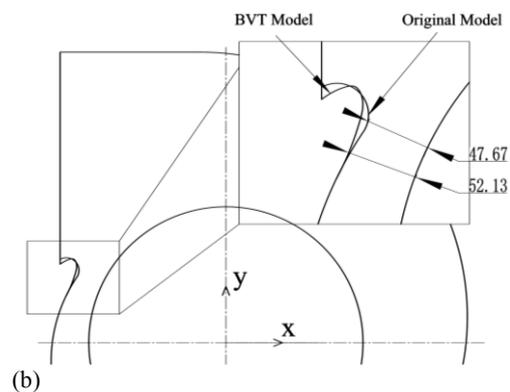
(b)

(c)

Fig. 7. Diagram of bionic volute tongue: (a) fitting line of leading-edge airfoil of the owl wing at 40% wingspan, (b) comparison of the original model and improved model volute tongue profile, (c) comparison of volute tongue profiles of BVT1, BVT2, and BVT3 models

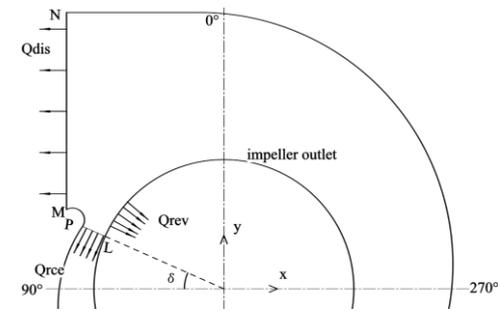## 5. IMPROVED EVALUATION METHOD FOR IMPELLER-VOLUTE TONGUE INTERACTION BASED ON UNSTEADY SIMULATION RESULTS

Wang *et al.* (2018) had proposed a two-dimensional evaluation method for impeller-volute tongue interaction, which introduced two parameters, namely the recirculated flow coefficient Q_{rec}/Q_{dis} and the reversed flow coefficient Q_{rev}/Q_{dis}. Here Q_{dis} refers to the discharge flow, which represents effective flow across the multi-wing centrifugal fan. Q_{rec} and Q_{rev} respectively represent the recirculated flow through the volute tongue clearance and the reversed flow back into the impeller from volute. It was also pointed out that the reduction of the recirculated flow coefficient and the reversed flow coefficient is conducive to improving the performance of the fan. Due to the limitations of analysis of the steady simulation results of previous research (Darvish and Frank 2012), an improved evaluation method base on unsteady simulation results has been proposed in this study. Since the physical time t plays a crucial role in the analysis process the discharge flow at time t is defined firstly
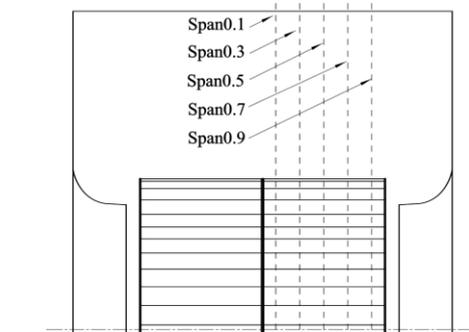
$$Q_{dis\_t} = \int_M^N -v_{x\_t}\,ds \tag{7}$$

Next, define the recirculated flow and reversed flow at time t.

$$Q_{rec\_t} = \int_L^P -(v_{x\_t}\_cos\theta + v_{y\_t}\_sin\theta)ds \tag{8}$$

$$Q_{rev\_t} = \int_0^{\pi/2} \frac{|v_{r\_t}(\theta)| - v_{r\_t}(\theta)}{4} D_2\,ds \tag{9}$$

where v_{x_t}, v_{y_t} are the horizontal and vertical velocity components of the airflow, M and N are the two boundary points of the discharge flow region, P and L are the two boundary points of the recirculated flow region, $v_{r\_t}(\theta)$ is the radial velocity of the impeller outlet at the θ degree position, and the angle δ showed in Fig. 8(a) is the installation angle of the volute tongue.
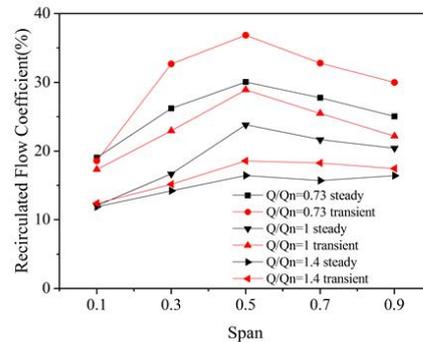
The unsteady simulation results at different times have been averaged. The average discharge flow, average recirculated flow, and average reversed flow are defined below

$$\overline{Q}_{dis} = \frac{1}{t}\sum_{t=1}^t Q_{dis\_t} \tag{10}$$

$$\overline{Q}_{rec} = \frac{1}{t}\sum_{t=1}^t Q_{rec\_t} \tag{11}$$

$$\overline{Q}_{rev} = \frac{1}{t}\sum_{t=1}^t Q_{rev\_t} \tag{12}$$

In the second section of this paper, it can be seen that the pressure is stable after five rounds of the impeller, so the unsteady simulation result of the sixth round is analyzed. As the impeller rotating 60°, an unsteady simulation result has been selected, denoted as t=1, 2...6. At the same time, six positions related to six different blade paths, which reduce the influence of position of blade path to the average result. Thus, the final expression of the recirculated flow coefficient and the reversed flow coefficient expression are $\frac{\overline{Q_{rec}}}{Q_{dis}}$ and $\frac{\overline{Q_{rev}}}{Q_{dis}}$, which are used in the following study.


(a)
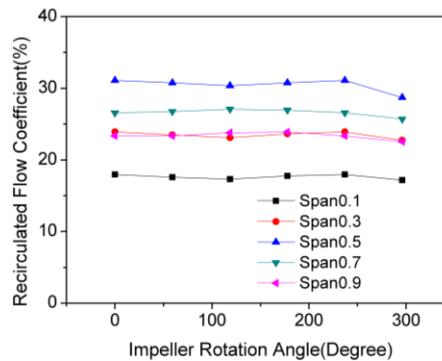
(b)

Fig. 9. Recirculated flow coefficient of origin fan: (a) recirculated flow coefficient of steady and unsteady simulation results, (b) recirculated flow coefficient of different rotation angle of impeller.

(a)

(b)

Fig. 8. Sketch of the upper part of the volute: (a) sketch of discharge and recirculation flow position, (b) selection of the spans.

After observing the flow field of the double suction fan, it is found that the flow field distribution is symmetrical with respect to the surface of impeller hub. Thus, the flowing analysis is performed on the fives spans on one side. The selections of spans are shown in Fig.8(b). The recirculated flow coefficient in different spans of the original model obtained in different flow rate between the steady and unsteady simulation results is shown in Fig. 9(a).It is found that the difference between the steady and unsteady simulation results is evident, which is more evident in the small flow rate condition.

Figure 9(b) shows the variation of the recirculated flow coefficient on different spans of the original fan at different stimulation time. It can be seen that the impeller rotation position is also the factor which affects the recirculation flow coefficient. Therefore, it is necessary to use the simulation results from unsteady simulation and the time average result to evaluate the impeller-volute tongue interaction.
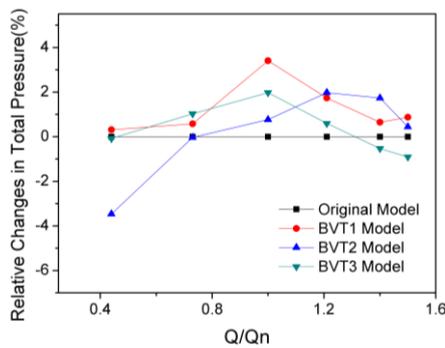
(a)
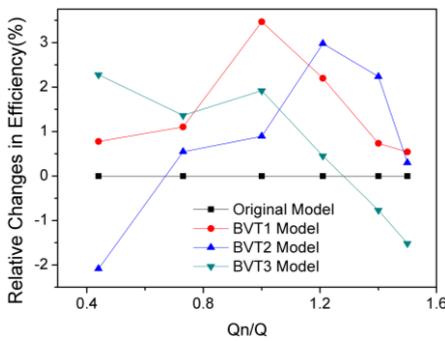
(b)

Fig. 10. Influence of different installation angles on the aerodynamic performance: (a) relative changes in total pressure, (b) relative changes in efficiency.

6. RESULTS AND DISCUSSIONS

6.1 Comparison of Aerodynamic Performance of the Fans

The improved models had been numerically simulated under six different flow rate conditions. The relative changes in total pressure of designed models are shown in Fig. 10 (a), and the relative changes in efficiency are shown in Fig. 10. (b).

It can be seen that the improved models present different performance at different flow rate conditions. The performance of BVT2 model with the volute tongue clockwise by 6°is the best in large flow rate conditions. While in small flow rate conditions, BVT3 model that the volute tongue counterclockwise by 6°is shows better performance. And BVT1 model presents improvement in performance under all operating conditions, especially in design condition.

6.2 Effect of Volute Tongue on flow Field

In order to reveal the internal mechanism of fan performance changes, the internal flow field of the fan has been further analyzed.

The airflow direction in the multi-blade centrifugal fan is changed from the axial in the inlet to the radial in the outlet (Breviario *et al*. 2016), which causes the distribution of airflow in the impeller and the distribution in volute is non-uniform in the axial direction. Thus, it is necessary to analyze the spanwise direction where airflow impacts obviously on volute tongue.

Figure 11 (a) shows the two sections Plane1 and Plane2 of the volute, which are used to investigate the axial flow of the airflow at the volute tongue. Figures 11(b) ~(e) show the streamlines in Plane1 and Plane2 under the flow condition of Q/Qn=0.73 and Q/Qn=1.4, where the streamlines and arrows indicate the direction of resultant velocity. The bottom of the figures is the volute region. It can be seen that the horizontal component of velocity at the middle position of the volute tongue is relatively small. In order to observe a more obvious impact phenomenon, the data of span0.15 is extracted to analyze in the following research.

In the flow rate of Q/Qn=1.4, the static pressure and streamline of the original model and the improved models in the 0.15 span are shown in Fig. 12. It can be observed that the change of the airflow direction near the volute tongue surface of the original model is more obvious, and the decrease of velocity leads to an increase in local static pressure. Thus, there is a broader static pressure mutation region of the original model. Figure 13 shows the static pressure distribution along the volute tongue. The static pressure value is higher in the region where the airflow impact is conspicuous observed in Fig. 11, which further embodies the connection between static pressure and impact phenomena.

In Fig. 12, the red line is used to segment the region where the airflow passes through the outlet of the volute and the region where the airflow flows back to the volute, which is called the stagnation line. The point of the stagnation line near the airfoil volute tongue is called the stagnation point. The stagnation points of the BVT1 and BVT2 models are close to the leading point of the airfoil profile. Thus, the velocity direction of the airflow near the volute tongue changes little, and the airflow is less obstructed by the volute tongue. The curvature radius of the original model volute tongue is relatively large, and the separation point of the BVT3 model is far from the leading point of the
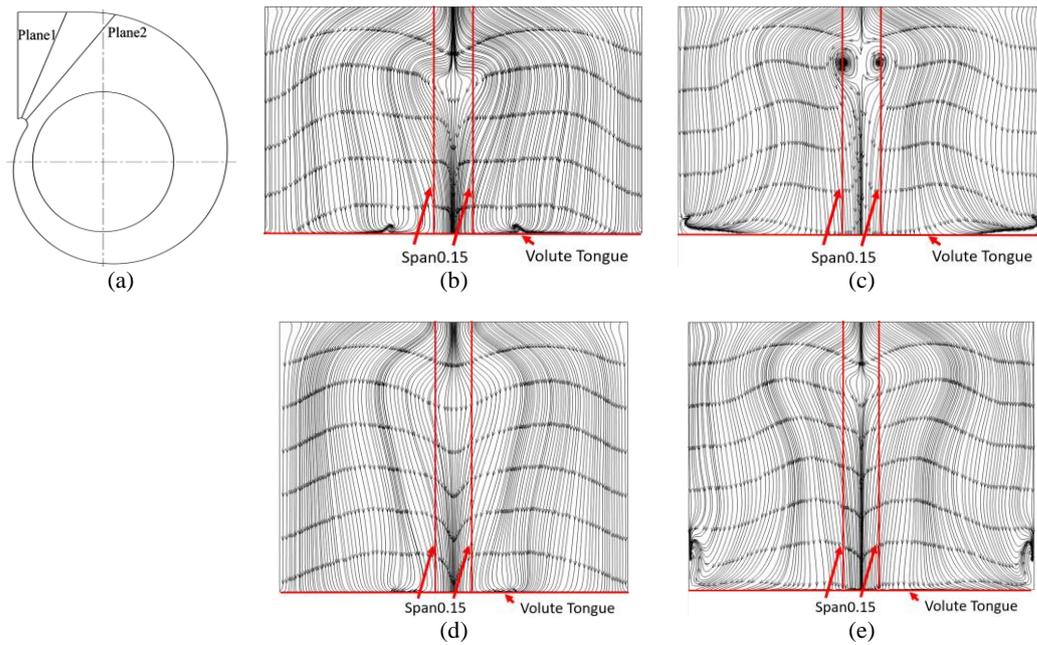
Fig. 11. Distribution of streamlines on the volute tongue: (a) selection of the planes, (b) streamlines in plane1 while the fan operates at Q/Qn=0.73, (c) streamlines in plane1 while the fan operates at Q/Qn=1.4, (d) streamlines in plane2 while the fan operates at Q/Qn=0.73, (e) streamlines in plane1 while the fan operates at Q/Qn=1.4.
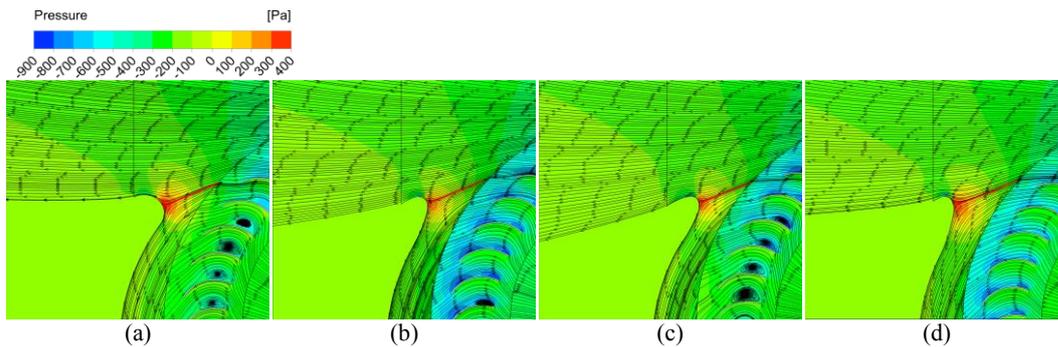
Fig. 12. Static pressure and streamlines in 0.15spanwhile fans operate at Q/Qn=1.4: (a) original fan, (b) BVT1 fan, (c) BVT2 fan, (d) BVT3 fan.
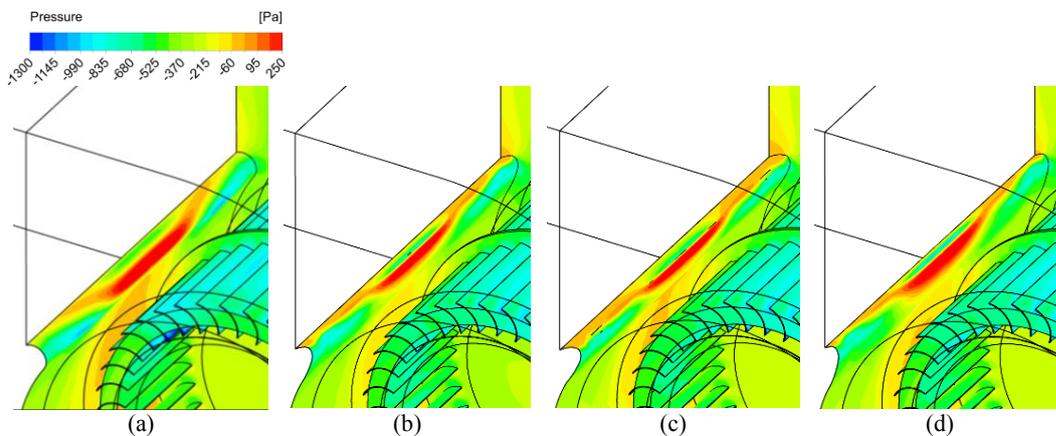
Fig. 13. Static pressure distribution of volute tongue while fans operate at Q/Qn=1.4: (a) original fan, (b) BVT1 fan, (c) BVT2 fan, (d) BVT3 fan.
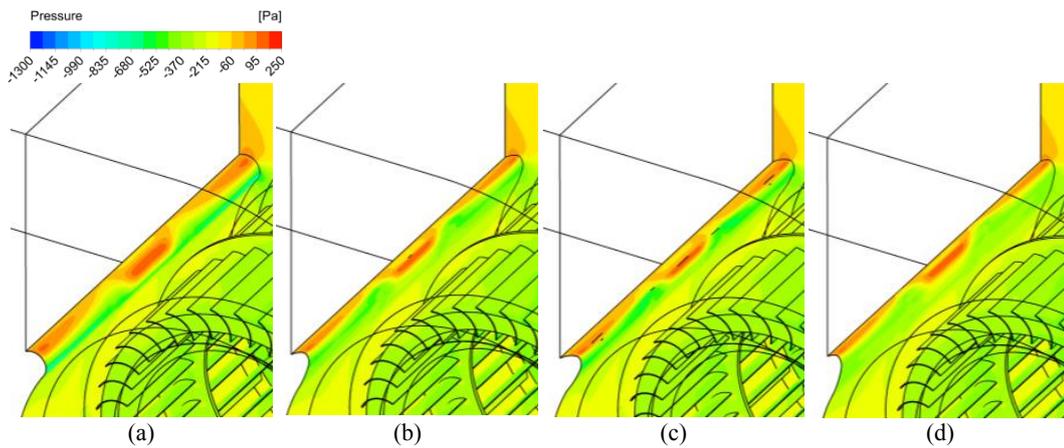
(a)   (b)   (c)   (d)
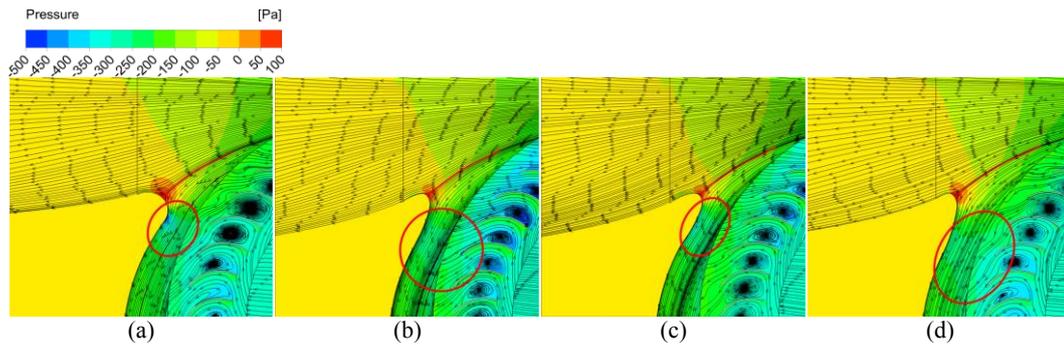
**Fig. 14. Static pressure and streamlines in 0.15 span while fans operate at Q/Qn=0.7: (a) original fan,
(b) BVT1 fan, (c) BVT2 fan, (d) BVT3 fan.**

(a)   (b)   (c)   (d)

**Fig. 15. Static pressure distribution of volute tongue while fans operate at Q/Qn=0.73: (a) original fan,
(b) BVT1 fan, (c) BVT2 fan, (d) BVT3 fan.**

airfoil, which makes the volute tongue have a more significant obstruction effect on the airflow and the energy loss caused by impact is also more substantial. Above, the reason why the aerodynamic performance of the original model and the BVT3 model is lower than that of BVT1 and BVT2 has been initially explained by the analysis of energy loss. It is worth noting that the area of static pressure mutation region of the BVT3 model is approximately the same as the original model, but the aerodynamic performance of the fan is reduced.

In the BVT1 and BVT2 models with larger volute gaps, the vorticity scale of the blade suction surface in the impeller domain is significantly reduced. It may be due to that the increase of the volute gap is effective for the dissipation of vortex at the blade suction surface.

At flow rate of Q/Qn=0.7,the static pressure and streamlines of the original model and the design models in the 0.15 span are shown in Fig. 14, and the static pressure distribution along the volute tongue are shown in Fig. 15.

Compared with the large flow rate condition, it can be seen that the stagnation line position on the flow rate of Q/Qn=0.73 has an upward moving, which reduces the flow incidence angle. Besides, the stagnation point of the BVT3 model with volute tongue inclined backward the impeller is closer to the leading point of the volute tongue than that at the

large flow rate condition. The area of pressure mutation region is significantly reduced in designed models, which shows the energy loss being decreased.

As shown indicated by the red circle in the figure, in the region of the volute tongue clearance, there are obvious pressure mutations of the original model and the BVT2 model. It shows that, for small flow rate conditions with insufficient airflow, an increase of length of volute tongue clearance can improve the flow stability at the region of volute tongue clearance. This observation may explain why the aerodynamic performance of the BVT3 and BVT1 models is improved in small flow rate conditions. In addition, it is worth noting that the aerodynamic performance of BVT3 model has unconspicuous improvement in flow rate condition Q/Qn=0.73.

In order to further explore the general mechanism, we have extracted and analyzed the surface pressure of the volute of the fan under the design flow condition, and selected three sections at span0.15, span0.5, and span0.85. Figure 16 shows the profile of the fan volute surface and the outlet of the fan. The analysis focuses on the tongue and spiral part of the volute. Figure 17 (a) (b) (c) shows the static pressure distribution of the fan volute. It can be seen that the application of the bionic volute tongue has little effect on the static pressure distribution of the spiral part of the volute.

In the part of the volute tongue, compared with the original model, the surface area of the volute that has a sharp change in pressure is significantly reduced, that is, the corresponding static pressure abrupt area is reduced, which is consistent with the observation of the volute pressure contour. Comparing the three design models, the pressure distribution on the left side of the volute span (span 0.15), The pressure is reduced successively forBVT2, BVT1 and BVT3, while in the right side of volute tongue in span0.85, the pressure is reduced successively for BVT3, BVT1 and BVT2. This is caused by the angle of incidence relative to the airfoil volute at different axial positions.

In general, finding a suitable angle of incidence is beneficial to reduce the flow loss at the volute tongue. The variation of the flow conditions changes the incident angle of the airflow, so the volute tongue with different inclination angles have different flow losses at the volute tongue under different flow conditions, which is one of the reasons that affect the aerodynamic performance of the fan.

However, by comparing the performance curves, two questions have been raised. It can be preliminary concluded that the length of the volute tongue clearance of BVT3 model is the largest of the four models, which can aggravate the recirculated flow that is not conducive to the improvement of the aerodynamic performance of the fan. In the next section of this chapter, we focus on the backflow of the volute tongue.
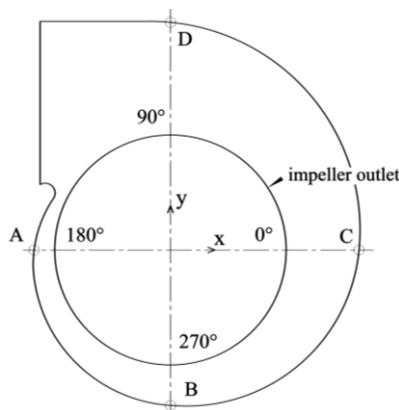

Fig. 16. Diagram of fan volute.

6.3 Recirculated flow Coefficient and Reversed flow Coefficient

In the fourth section, the feasibility and necessity of the improved evaluation method of internal flow circulation based on unsteady simulation results are verified. Next, the effects of the volute tongue installation angle on the recirculated flow coefficient and reversed flow coefficient of the volute of the fan are compared and analyzed.

Figure 18 shows the recirculated flow coefficients in the different spans of the original and designed models under different flow conditions. In the design flow rate condition and the large flow rate condition, the value of the recirculated coefficients is positively correlated with the length of volute tongue clearance. In small flow condition, the values of recirculated flow coefficients of four models near the wheel hub are basically the same. However, as the increase of clearance length, the values of recirculated flow coefficients of spans where close to the wheel shroud still increases. This means that an increase of the length of volute tongue clearance does increase the recirculated flow. This is why the aerodynamic performance of the BVT3 model deteriorated in large flow rate conditions and improved slightly in small flow conditions. At this point, the two questions raised previously have been explained.

Further, Fig. 19 shows the reversed flow coefficient for the different spans of the four models under different flow rate conditions, which is also a critical coefficient to evaluate the impeller-volute tongue interaction. It can be found that the reversed flow coefficient close to the impeller wheel hub is small. Moreover, in design conditions and large flow conditions, there is less than 15% reversed flow only near the impeller wheel shroud. The main reason for this phenomenon is the existence of secondary vortices near the impeller wheel shroud, which can be observed by observing the streamline of the meridian plane (Wen *et al*. 2013; Wright *et al*. 1984).In the small flow condition, the air is unable to fill the whole the blade passages, which causes the increase of reversed flow. Thus, it leads to the reversed flow coefficient overall high.

It can be seen that the application of the bionic volute tongue has no effect on the reduction of the reversed flow coefficient under the design condition. In addition, the reversed flow of the BVT2 model increases slightly in some specific spans under non-design flow rate condition, which may be due to the obvious impeller-volute tongue interaction for the small distance between impeller and volute tongue. It can be considered that, due to the change of the volute gap, the variation of the recirculated flow has a greater impact on the fan performance than the reversed flow.

In summary, the increase of circulated flow in BVT3 model is due to its volute clearance extension. This leads to poor performance under large flow conditions and the insignificant improvement in aerodynamic performance under small flow conditions. In the design of a fan, choosing a reasonable installation angle, reducing the flow energy loss at the volute and improving the inflow circulation caused by the volute are important factors to obtain better aerodynamic performance of fans.

7. CONCLUSIONS

In this study, the profile of the leading edge of the owl wing was applied to improve the design of the volute tongue of the double-suction multi-blade centrifugal fan. The fan models with different volute tongue installation angles were numerically simulated, and the aerodynamic performances were compared. The influence of different installation angles of the volute tongue on the aerodynamic
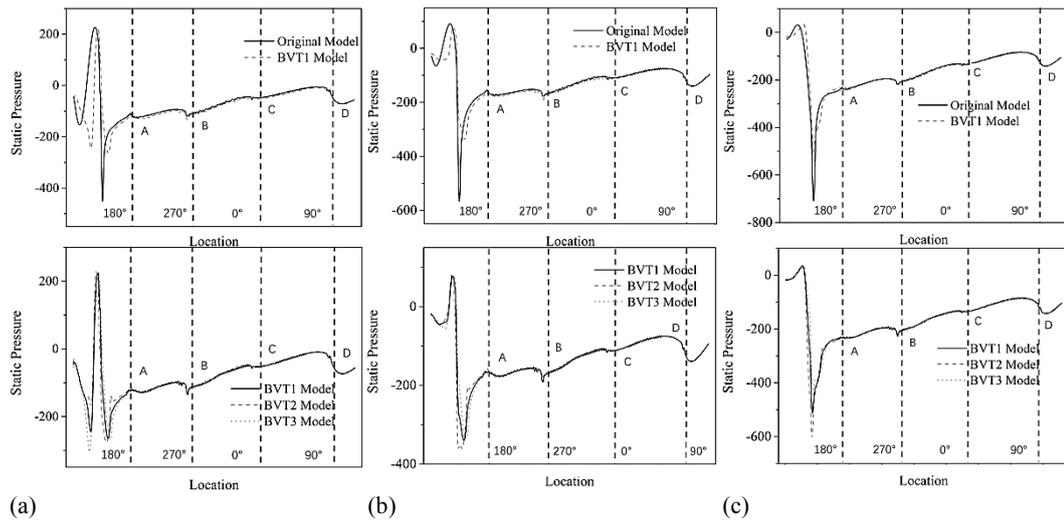
Fig. 17. Pressure distribution on the surface of volute in different spans while fans operate at Q/Qn=1:
(a) span0.15, (b) span0.5, (c) span0.85.
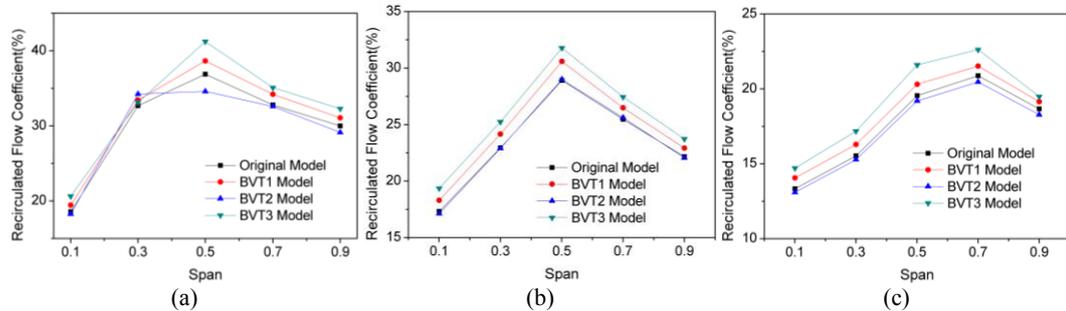
Fig. 18. Recirculated flow coefficient of original model and BVT models indifferent flow rate: (a)
Q/Qn=0.73; (b) Q/Qn=1; (c) Q/Qn=1.4.
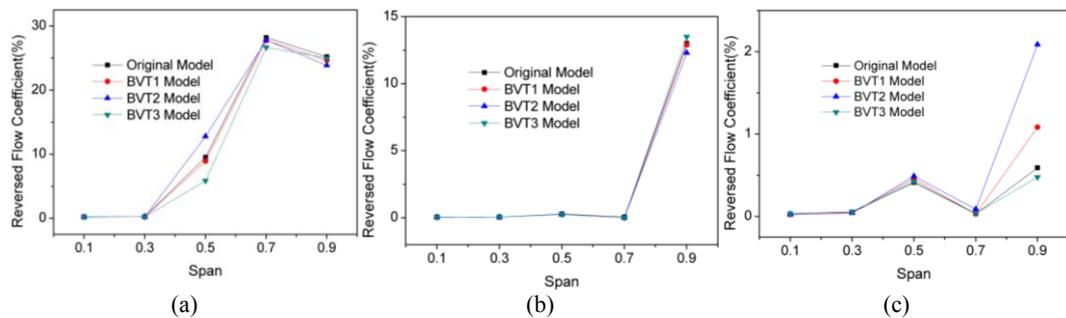
Fig. 19. Reversed flow coefficient of original model and BVT models indifferent flow rate: (a)
Q/Qn=0.73; (b) Q/Qn=1; (c) Q/Qn=1.4.

performance of the fan are discussed in terms of energy loss at the volute tongue and the internal flow circulation of the volute. The following conclusions had been mainly drawn:

1. In terms of the aerodynamic performance, the volute tongue that inclines toward impeller is beneficial to the improvement of the aerodynamic performance of the fan under large flow rate condition, and the volute tongue that inclines backward has a better performance under small flow rate condition. While the volute tongue without inclined performs best in the design condition.

2. The application of the bionic volute tongue can

improve the flow quality at the tip of the volute tongue. The position of separation point at the volute tongue varies as the flow conditions change. By changing the installation angle of the volute tongue, the closer the airflow separation point to the leading point of the airfoil volute tongue, the smaller the change of the airflow velocity direction at the volute tongue. This leads to the smaller of the area of static pressure mutation and the less energy loss at the volute tongue. However, the increase of the length of volute tongue clearance can improve the flow stability of the region of volute tongue clearance at low flow rate condition.

3. An improved method for quantitatively evaluating

the level of impeller-volute tongue interaction is proposed in this study. This method can be used feasibly and effectively to analyze the unsteady simulation results. The physical meaning of the coefficient is the ratio of the circulating flow to the effective flow at the outlet. The increase of the length of the volute tongue clearance can increase the recirculated flow coefficient, which is not conducive to the improvement of the aerodynamic performance of the fan.

REFERENCES

Bouhelal，A., A. Smaili, O. Guerri and C. Masson (2018). Numerical investigation of turbulent flow around a recent horizontal axis wind turbine using low and high Reynolds models. *Journal of Applied Fluid Mechanics* 11 (1), 151-164.

Breviario, F., D. Brivio, L. Cardillo, A. Corsini and G. Delibra (2016). Flow survey of a forward curved blades centrifugal fan for HVAC applications. *Proceedings of ASME Turbo Expo 2016: Turbomachinery Technical Conference and Exposition*, Seoul, South Korea.

Cheng, X. D (2011). Impeller pump ventilator compressor. *Beijing: China Mechanical Industrial Pre.* (in Chinese).

Darvish, M. and S. Frank (2012). *Toward the CFD simulation of sirocco fans: from selecting a turbulence model to the role of cell shapes*. Fan 2012, Senlis, France.

Dong, J. and D. F. Li (2020). A reliable second-order hydrostatic reconstruction for shallow water flows with the friction term and the bed source term. *Journal of Computational and Applied Mathematics* 376,112871.

Gou, E. M. and K. Y. Kim (2003). Three-dimensional flow analysis and improvement of slip factor model for forward-curved blades centrifugal fan. *Journal of Mechanical Science and Technology* 18(2), 302-312.

Graham, R. R (1934).The silent flight of owls. *Aeronautical Journal* 10(38), 837-843.

Kawaguchi, K., S. Kadota, M. Suzuki, M. K. Kazuma and Kikuyama (1994). Experimental study on noise reduction of multiblade fan. 2nd report, relation of flow between fan blades and pressure fluctuations. *Transactions of the Japan Society of Mechanical Engineers, Part B JSME: Ser B* 60(570), 458-46.

Kind, R. J. and M. G. Tobin (1990). Flow in a Centrifugal Fan of the Squirrel Cage Type. *ASME Journal of Turbomachinery* 112(1), 84-90.

Klan, S., T. Bachmann, M. Klaas, H. Wagner and W. Schröder (2009). Experimental analysis of the flow field over a novel owl based airfoil. *Experiments in Fluids* 46(5), 975-989.

Li, D. and X. Liu (2016). Aerodynamic performance and acoustic characteristics of bionic airfoil inspired by three-dimensional long-eared owl wing under low Reynolds number. *Proceedings of ASME Turbo Expo 2016: Turbomachinery Technical Conference and ExpositionGT2016*, Seoul, South Korea.

Li, K., X. Chen, H. S. Dou, Z. Zhu, L. Zheng and X. Luo (2019). Study of flow instability in a miniature centrifugal pump based on energy gradient method, *Journal of Applied Fluid Mechanics* 12(3), 701-713.

Liu, T. S., K. Kuykendall, R. Rhew and S. Jones (2006). Avian wing geometry and kinematics. *AIAA Journal* 44(5), 954-963.

Liu, X. M. and S. Li (2015). Effects of bionic volute bioinspired by leading edge of owl wing on aerodynamic performance and noise of multi-blade centrifugal fan. *Journal of Xi'an Jiaotong University* 39(7), 14-21 (in Chinese).

Peng, G., Z. Gao and X. Feng (2020). An extremum-preserving finite volume scheme for convection-diffusion equation on general meshes. *Applied Mathematics and Computation* 380, 125301.

Sun, S. M. (2008). Coupling bionic research on the aerodynamic noise controlling of aerodynamic turbine. *PhD Thesis, Changchun, University of Jilin* (in Chinese).

Sun, S. M., L. Q. Ren, T. Mei, Y. Z. Zhang and Z. H. Qian (2009). Practice and simulation analysis for reducing the centrifugal fan noise with bionics volute tongue .*Journal of Vibration and Shock* 28(5), 32-34.

Supreeth, R., A. Arokkiaswamy, K. Anirudh, R. K. Pradyumna, P. K. Pramod and A. K Sanarahamat (2020). Experimental and numerical investigation of the influence of leading edge tubercles on S823 airfoil behavior, *Journal of Applied Fluid Mechanics* 13(6), 1885-1899.

Wang, K., Y. P. Ju and C. H. Zhang (2017).Design of multi-blade centrifugal fan based on grouping model and bionic volute tongue. *Journal of Engineering Thermophysics* 38(8), 1671-1675 (in Chinese).

Wang, K., Y. P. Ju and C. H. Zhang (2018).A quantitative evaluation method for impeller volute tongue interaction and application to squirrel. *Journal of Fluids Engineering* 141(8), 2-30.

Wang, K., Y. P. Ju and C. H. Zhang (2019). Numerical investigation on flow mechanisms of squirrel cage fan. *Journal of Power and Energy* 233(1), 3-16.

Wang, M. and X. Liu (2019). Numerical investigation of aerodynamic and acoustic characteristics of bionic airfoils inspired by bird wing. *Proceedings of the Institution of Mechanical Engineers, Part G: Journal of Aerospace Engineering* 11(233), 4004-4016.

Wen, X. F., D. T. Qi, Y. J. Mao and Y. Xin (2013). Experimental and numerical study on the inlet nozzle of a squirrel-cage fan. *Journal of Power and Energy* 227(4): 450-463.

Wright, T. (1984). Centrifugal fan performance with inlet clearance. *Journal of Engineering for Gas Turbines and Power* 10(106), 906-912.